AD_____

Award Number: DAMD17-02-1-0358

TITLE: Monitoring Cancer Oxygenation Changes Induced by Ultrasound

PRINCIPAL INVESTIGATOR: Daqing Piao, Ph.D.
Quing Zhu, Ph.D.

CONTRACTING ORGANIZATION: University of Connecticut
Storrs, Connecticut 06269-4133

REPORT DATE: July 2004

TYPE OF REPORT: Annual Summary

PREPARED FOR: U.S. Army Medical Research and Materiel Command
Fort Detrick, Maryland 21702-5012

REPORT DOCUMENTATION PAGE

Form Approved
OMB No. 074-0188

1. AGENCY USE ONLY (Leave blank)	2. REPORT DATE	3. REPORT TYPE AND DATES COVERED
	July 2004	Annual Summary (15 Jun 03 - 14 Jun 04)

4. TITLE AND SUBTITLE
Monitoring Cancer Oxygenation Changes Induced by Ultrasound

5. FUNDING NUMBERS
DAMD17-02-1-0358

6. AUTHOR(S)
Daqing Piao, Ph.D.
Quing Zhu, Ph.D.

7. PERFORMING ORGANIZATION NAME(S) AND ADDRESS(ES)
University of Connecticut
Storrs, Connecticut 06269-4133

E-Mail: piao@engr.uconn.edu

8. PERFORMING ORGANIZATION REPORT NUMBER

9. SPONSORING / MONITORING AGENCY NAME(S) AND ADDRESS(ES)
U.S. Army Medical Research and Materiel Command
Fort Detrick, Maryland 21702-5012

10. SPONSORING / MONITORING AGENCY REPORT NUMBER

11. SUPPLEMENTARY NOTES

12a. DISTRIBUTION / AVAILABILITY STATEMENT
Approved for Public Release; Distribution Unlimited

12b. DISTRIBUTION CODE

13. Abstract *(Maximum 200 Words)* ***(abstract should contain no proprietary or confidential information)***

Oxygen has significant impact on cancer treatment. Our hypothesis was: (a) Tumor blood vessels were leaky and therefore acoustic vibration can be used to modulate the leaky vessels and induce oxygenation changes; (b) The oxygenation changes can be detected by optical measurements. Preliminary studies with 5 tumor-bearing rats demonstrate that ultrasonic vibrations can either generate significant effects (early stage tumors) on optical measurements or no effects on optical measurements (late stage tumors). In the past year, the PI has devoted his efforts on quantify both acoustic vibration and optical measurement of oxygenation: (1) Optimization of ultrasound system for quantification of mechanical stress generated by the ultrasound vibration (in task 2); (2) Optimization of optical wavelength selection for in vivo oxygenation estimation (in tasks 1 and 3).

14. SUBJECT TERMS
Cancer therapy, cancer hypoxia, optical spectroscopy, ultrasound contrast agent

15. NUMBER OF PAGES
9

16. PRICE CODE

17. SECURITY CLASSIFICATION OF REPORT	18. SECURITY CLASSIFICATION OF THIS PAGE	19. SECURITY CLASSIFICATION OF ABSTRACT	20. LIMITATION OF ABSTRACT
Unclassified	Unclassified	Unclassified	Unlimited

Table of Contents

INTRODUCTION:

It is well known that oxygen has significant impact on cancer treatment. Our hypothesis for this research was: (a) Tumor blood vessels were leaky and therefore acoustic vibration can be used to modulate the leaky vessels and induce oxygenation changes; (b) The oxygenation changes can be detected by optical measurements. Preliminary studies with 5 tumor-bearing rats demonstrate that ultrasonic vibrations can either generate significant effects (early stage tumors) on optical measurements or no effects on optical measurements (late stage tumors). During the past year, the PI has devoted his efforts on quantify both acoustic vibration and optical measurement of oxygenation.

BODY:

1. Optimization of ultrasound system for quantification of mechanical stress generated by the ultrasound vibration (in task 2)

The ultrasound system that the PI used to conduct the preliminary animal experiments was transmission only. The acoustic pulses of various energy levels were delivered to the tumors and the acoustic induced effects were measured optically. However, the optical measurements were not directly proportional to the acoustic energy and were significantly modulated by the tumor elastic condition. This is probably why we observed significant changes for two early-stage tumor rats but no changes for two late stage tumor rats.

To directly measure ultrasonic pressure effects, we have constructed the 64-channel receiving ultrasound system. The system is designed for real-time RF data acquisition, which can be used to calculate the mechanical strain generated at tumor spot.

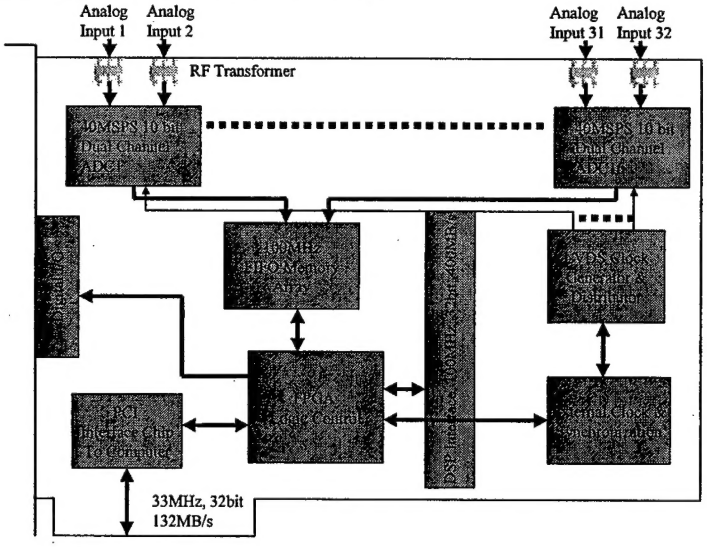

Fig. 1. Block diagram of a single PCI DAQ card

The 64-channel data acquisition system includes two identical standard full-length PCI DAQ cards for personal computers. Each PCI DAQ accepts 32-channel analog inputs and digitizes all the inputs simultaneously at a rate of 40MSPS, 10bit. The block diagram of a single PCI DAQ card is shown in Fig. 1. For each PCI DAQ card, 32-channel analog inputs are digitized by 16 dual-channel 40MSPS, 10bit ADCs MAX1186 (Maxim Inc). Digitized RF data are stored in a 160bit wide, 100MHz FIFO memory array. The RF data can be transferred to host computer at a data transfer rate of 132MB/s through a PLX9054 (PLXTECH, Inc) PCI interface chip when operating at DMA mode, or to external DSP board at a data transfer rate of 400MB/s for process. Three Altera FPGAs are used to interface with PCI interface chip, external DSP board, external digital I/O lines and external clock and

synchronization. An LVDS (Low Voltage Differential Signaling) clock generator and distributor network are implemented to provide very accurate, noise-immune and jitter-free clocks to all ADC channels. In PCB (printed circuit board) layout, cares are taken to provide a constant impedance, equal-length traces of ADC clock signals to ensure accurate phase uniformity when digitizing all 32 analog channels. Proper analog/digital ground separation and wide band input RF transformers are used to provide ground isolation and reduce digital noise and cross-talk between analog channels. The photography of the data acquisition card is shown in Fig.2. Currently, the system hardware construction and testing are completed and the efforts are devoted to software debugging and implementing strain estimation algorithm.

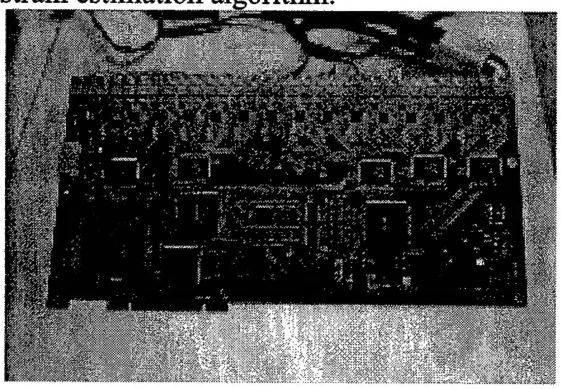

Fig.2. Photo of the data acquisition card that will be used to estimate ultrasonically generated stain, which may induce tumor oxygenation changes

2. Optimization of optical wavelength selection for *in vivo* oxygenation estimation (in tasks 1 and 3)

The optical measurements observed in preliminary rat tumor studies were simply amplitude changes and quantitative oxygenation calculation is needed to evaluate the proposed methods.

Literature data regarding to optimal optical wavelength for tumor hemoglobin concentration and oxygen calculation are very confusing. Many research groups have constructed multi-wavelength systems using either frequency domain or time-resolved approach [1-2]. The total number of wavelengths deployed in the reported systems has been increased dramatically in recent years varying from 3 to 9 optical wavelengths. With more wavelengths, the wavelength-dependent tumor absorption changes can be obtained. However, the computation of total hemoglobin and hypoxia distributions requires an optimal set of wavelengths. Furthermore, the data acquisition time will increase dramatically with the increasing wavelengths. Recently, the PI worked with other Ph.D. students in the Lab have constructed a frequency domain system consisting three wavelengths of 660nm, 780 nm and 830 nm [3].

Are these three wavelengths good enough to accurately and robustly compute the hemoglobin concentration and oxygenation from optical measurements? The PI has analyzed this problem from both theory and practice. The analysis is as follows.

By assuming that the major chromophores are deoxygenated (deoxyHb) and oxygenated (oxyHb) hemoglobin in the wavelength range studied, we can estimate deoxyHb and oxyHb concentrations at each imaging voxel by inverting the following equations

$$\begin{bmatrix} \mu_a^{\lambda_1}(r') \\ \mu_a^{\lambda_2}(r') \end{bmatrix} = \begin{bmatrix} \varepsilon_{Hb}^{\lambda_1}, \varepsilon_{HbO_2}^{\lambda_1} \\ \varepsilon_{Hb}^{\lambda_2}, \varepsilon_{HbO_2}^{\lambda_2} \end{bmatrix} \times \begin{bmatrix} deoxyHb(r') \\ oxyHb(r') \end{bmatrix}, \quad (1)$$

and obtain deoxyHb and oxyHb as:

$$\begin{bmatrix} deoxyHb(r') \\ oxyHb(r') \end{bmatrix} = \frac{1}{\Delta}\begin{bmatrix} \varepsilon_{HbO_2}^{\lambda_2}, -\varepsilon_{HbO_2}^{\lambda_1} \\ -\varepsilon_{Hb}^{\lambda_2}, \varepsilon_{Hb}^{\lambda_1} \end{bmatrix} \times \begin{bmatrix} \mu_a^{\lambda_1}(r') \\ \mu_a^{\lambda_2}(r') \end{bmatrix}. \tag{2}$$

The total hemoglobin concentration $totalHb(r') = deoxyHb(r') + oxyHb(r')$ and oxygenation saturation $Y\% = \dfrac{oxyHb(r')}{oxyHb(r') + deoxy(r')} 100\%$ can be calculated as:

$$totalHb(r') = \frac{1}{\Delta}\left\{\{\varepsilon_{HbO_2}^{\lambda_2} - \varepsilon_{Hb}^{\lambda_2}\}\mu_a^{\lambda_1}(r') + \{\varepsilon_{Hb}^{\lambda_1} - \varepsilon_{HbO_2}^{\lambda_1}\}\mu_a^{\lambda_2}(r')\right\} \tag{3}$$

and

$$Y\% = \frac{-\varepsilon_{Hb}^{\lambda_2}\dfrac{\mu_a^{\lambda_1}(r')}{\mu_a^{\lambda_2}(r')} + \varepsilon_{Hb}^{\lambda_1}}{(\varepsilon_{HbO_2}^{\lambda_2} - \varepsilon_{Hb}^{\lambda_2})\dfrac{\mu_a^{\lambda_1}(r')}{\mu_a^{\lambda_2}(r')} - (\varepsilon_{HbO_2}^{\lambda_1} - \varepsilon_{Hb}^{\lambda_1})} 100\%, \tag{4}$$

where $\Delta = \varepsilon_{Hb}^{\lambda_1}\varepsilon_{HbO_2}^{\lambda_2} - \varepsilon_{HbO_2}^{\lambda_1}\varepsilon_{Hb}^{\lambda_2}$. In principle, any two wavelengths in the NIR window can be used to compute the total hemoglobin concentration from equation (3). However, positive coefficients of $\mu_a^{\lambda_1}(r')$ and $\mu_a^{\lambda_2}(r')$ in equation (3) are critical to guarantee that the estimated total hemoglobin concentration at each voxel is positive, especially in the background region where the absorption coefficients are small and consequently the relative estimation errors of absorption coefficients are larger that those in the lesion region. The second practical consideration is the sensitivity of the total hemoglobin concentration to estimation errors of $\mu_a^{\lambda_1}(r')$ and $\mu_a^{\lambda_2}(r')$. The sensitivity is defined as the partial derivatives of totalHb to $\mu_a^{\lambda_1}(r')$ and $\mu_a^{\lambda_2}(r')$, which are given as:

$$\frac{\partial totalHb(r')}{\partial \mu_a^{\lambda_1}(r')} = \frac{1}{\Delta}\left\{\{\varepsilon_{HbO_2}^{\lambda_2} - \varepsilon_{Hb}^{\lambda_2}\}\right\}, \frac{\partial totalHb(r')}{\partial \mu_a^{\lambda_2}(r')} = \frac{1}{\Delta}\left\{\{\varepsilon_{Hb}^{\lambda_1} - \varepsilon_{HbO_2}^{\lambda_1}\}\right\}. \tag{5}$$

If a wavelength after isobestic point is chosen as λ_2, for example 830 nm, the coefficient $\frac{1}{\Delta}\left\{\{\varepsilon_{HbO_2}^{\lambda_2} - \varepsilon_{Hb}^{\lambda_2}\}\right\}$ of $\mu_a^{\lambda_1}(r')$ is positive as shown in Fig. 3 (circled line), however, the coefficient $\frac{1}{\Delta}\left\{\{\varepsilon_{Hb}^{\lambda_1} - \varepsilon_{HbO_2}^{\lambda_1}\}\right\}$ of $\mu_a^{\lambda_2}(r')$ is positive only for wavelength $\lambda_1 < 798$ nm (* line). The extinction coefficients used for calculation were obtained from Ref. [ph.d dissertation] in a natural logarithmic scale with units of inverse millimoles times inverse centimeters. However, the sensitivity of total hemoglobin estimation to $\mu_a^{\lambda_2}(r')$ for $\lambda_1 < 780$ nm is much higher than that of $\mu_a^{\lambda_1}(r')$. The best equal sensitivity wavelength range of λ_1 for given $\lambda_2 = 830$ nm is between 780 nm and 785 nm.

Similarly, any two wavelengths in the NIR window can be used to compute the oxygenation saturation from equation (4). However, the sensitivity of Y% to ratio $\frac{\mu_a^{\lambda_1}(r')}{\mu_a^{\lambda_2}(r')}$ is significantly different for different wavelength pairs. Figure 4 plots the Y% vs. the ratio for wavelength pairs (660nm, 830nm, circles), (710 nm, 830nm, starts) and (780nm, 830nm, crosses). For the first two pairs, the Y% lies in the physiology range for $\frac{\mu_a^{\lambda_1}(r')}{\mu_a^{\lambda_2}(r')} > 0.2$. However, for the wavelength pair of (780 nm, 830nm), the Y% is greater than 100% for $\frac{\mu_a^{\lambda_1}(r')}{\mu_a^{\lambda_2}(r')} < 0.7$ and reduces quickly to zero for ratio > 1.4. Therefore, any estimation error on $\mu_a^{\lambda_1}(r')$ and $\mu_a^{\lambda_2}(r')$ can cause the Y% out of the expected physiology range, particularly when the $\mu_a^{\lambda_1}(r')$ and $\mu_a^{\lambda_2}(r')$ are small in the background tissue regions or $\mu_a^{\lambda_1}(r')$ and $\mu_a^{\lambda_2}(r')$ are large in the malignant cancer regions. This was exactly the problem that we had with our first frequency domain system where the wavelength pair of (780nm, 830nm) was used.

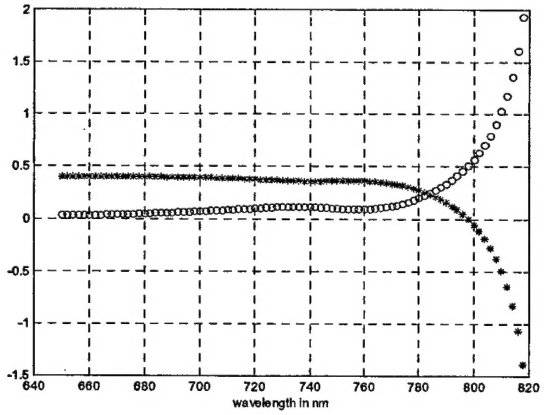

Fig.3. The coefficient $\frac{1}{\Delta}\left\{\{\varepsilon_{HbO_2}^{\lambda_2} - \varepsilon_{Hb}^{\lambda_2}\}\right\}$ of $\mu_a^{\lambda_1}(r')$ is positive as shown by circled line, however, the coefficient $\frac{1}{\Delta}\left\{\{\varepsilon_{Hb}^{\lambda_1} - \varepsilon_{HbO_2}^{\lambda_1}\}\right\}$ of $\mu_a^{\lambda_2}(r')$ is positive only for wavelength $\lambda_1 < 798$ nm (see * line).

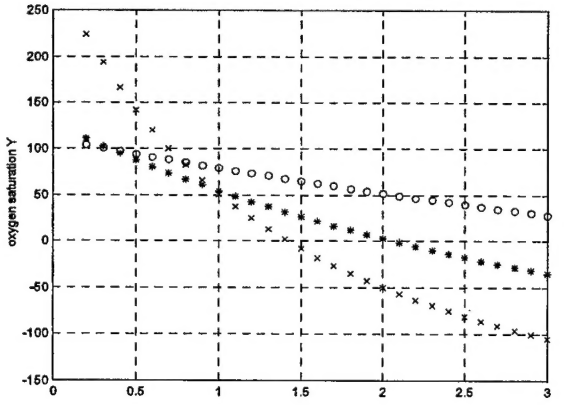

Fig. 4. Oxygen saturation (Y%) vs. the ratio for wavelength pairs (660nm, 830nm, circles), (710 nm, 830nm, starts) and (780nm, 830nm, crosses). Both pairs of (660nm, 830nm) and (710nm, 830) are acceptable.

Therefore, to ensure equal sensitivity of total hemoglobin concentration estimation to two wavelengths, the wavelength pair of (780 nm, 830 nm) is optimal; while to ensure robust oxygenation saturation estimation, the wavelength pair of (660nm, 830) is optimal. As a result, three typical wavelengths of 660nm, 780nm, and 830nm are required for total hemoglobin and oxygen saturation.

Figure 5 shows results obtained from a human breast cancer using the optimal wavelengths discussed. Fig.5. (a)-(c) are ultrasound images of the breast cancer under chemotherapy treatment acquired before treatment, during treatment and after six cycles of treatment. This example is attended to demonstrate the use of optimal wavelength and the algorithms to calculate the total hemoglobin concentration and oxygen saturation. (d), (e) and (f) are corresponding optical hemoglobin concentrations acquired at the same time as the ultrasound images. (g), (h) and (i) are oxygen saturation maps. The slices in (d)-(i) are numbered from left to right and top to bottom. Slice 1 is 0.5cm deep into the breast and slice 7 is 3.5 cm toward the chest wall. The oxygen saturation value is within the physiological range. Currently, we are preparing manuscript of this work for publication.

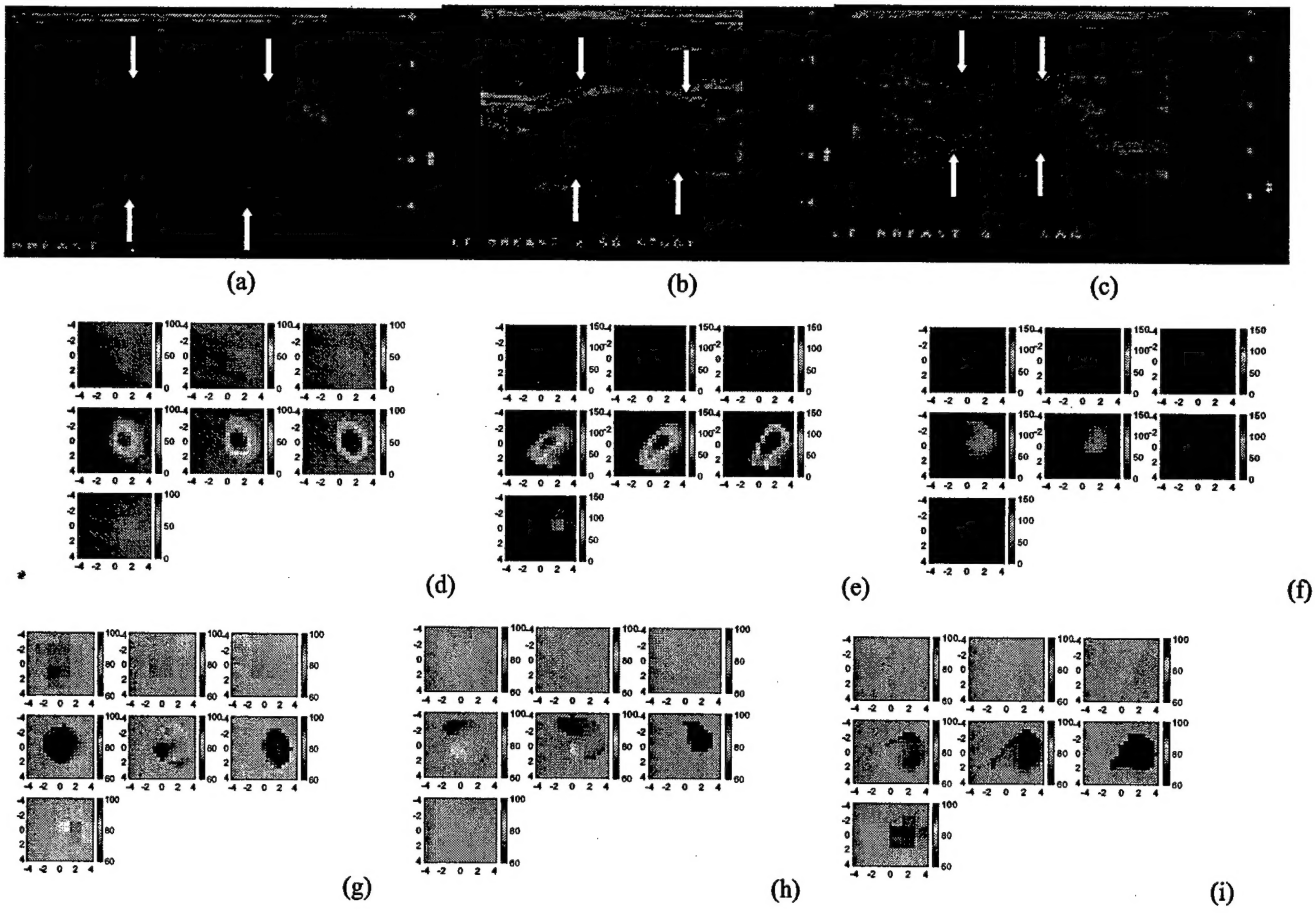

Fig.5. (a)-(c) ultrasound images of a human breast cancer under chemotherapy treatments. (d), (e) and (f) are corresponding optical hemoglobin concentrations acquired at the same time as the ultrasound images(g), (h) and (i) are oxygen saturation maps. The slices in (d)-(i) are numbered from left to right and top to bottom. Slice 1 is 0.5cm deep into the breast and slice 7 is 3.5 cm toward the chest wall.

KEY RESEARCH ACCOPLISHMENTS:

- Constructed a 64-channel receiving ultrasound system for the quantification of mechanical stress generated by the ultrasound vibration
- Investigated the theoretical basis of using three wavelengths to compute the hemoglobin concentration and oxygenation from optical measurements.
- Conducted *in vivo* study to validate using three wavelengths to compute the hemoglobin concentration and oxygenation

REPORTABLE OUTCOMES:

- A journal paper titled as "Robust estimation of tumor hemoglobin and oxygenation saturation distributions" is in preparation based on the work reported here.

CONCLUSIONS:

I have successfully finished Task 2 specified in the statement of my proposal. I have built a 64-channel receiving ultrasound system to optimize the ultrasound instrument, and have developed detailed analysis and algorithm on robust estimation of tumor Hemoglobin and oxygenation saturation distributions.

REFERENCES:

[1] H. Dehghani, B. Pogue, S.P. Poplack, and K.D. Paulsen, "Multiwavelength three-dimensional near-infrared tomography of the breast: initial simulation, phantom, and clinical results," Appl. Opt., **42 (1)**, 135-145 (2003).

[2] N.G. Chen, and Q. Zhu, "Time-resolved diffusive optical imaging using pseudo-random bit sequences," Opt. Expr., **11**, 3445-3454 (2003).

[3] M. Cope, Ph.D Dissertation, University of College London, 1991.